Chapter 7
Rotordynamic Influence of Balance Pistons with Combined Axial and Radial Flow

Maximilian M.G. Kuhr, Zhengzhong Gao, and Peter F. Pelz

Abstract The dynamic behaviour of rotating machinery, such as compressors or turbo pumps, is largely influenced by the dynamic characteristics of narrow fluid-filled gaps, namely media- or oil-lubricated journal bearings, annular seals, thrust bearings and balance pistons. In addition to the induced forces and moments on the rotor due to the hydrodynamic effect, the specific machine elements are subjected to substantial pressure differences, resulting in considerable axial, radial, or combined axial and radial flow components, as seen for example in balance pistons. While the rotordynamic force characteristic of narrow gaps, such as conventional journal bearings or annular seals, and its rotordynamic impact is well-documented, the rotordynamic influence of machine elements inducing forces and moments - like long seals and bearings, balance pistons, or thrust balancers - is less understood. To better comprehend the dynamics of such narrow gaps, the revision of an existing test rig at the Chair of Fluid Systems at the Technische Universität Darmstadt is presented. During the revision, a comprehensive rotordynamic analysis was carried out using Finite Element Method (FEM) simulations. The objective was to identify safe operating conditions concerning the natural frequencies and stability of the rotor, and to assess the influence of the fluid-filled annuli on the overall rotordynamic characteristic of the test rig. In particular, the influence of different degrees of modelling of the rotordynamic influence of the fluid-filled gaps was investigated. Specifically, the influence of the added mass, as well as the additional stiffness and damping resulting from either the induced forces or moment due to the translational and angular degrees of freedom, was examined. It is shown that in contrast to the classical assumption of solely assuming induced forces, the additional tilt and moment coefficients highly influence the stability of the overall system as well as the specific natural frequencies of certain vibrations modes.

Keywords Rotordynamics · Narrow gaps · FEM

Introduction

In the context of contemporary turbomachinery design and development, there is a notable emphasis on the pursuit of enhanced operational capabilities, elevated rotational speeds, and the reduction of overall machinery weight. These developments are driven by the demand for more efficient and compact machines that can operate in a wider range of conditions. However, these innovations present specific technical challenges, particularly in relation to the emergence of complex vibrational behaviour, which is difficult to predict and control. These vibrations are even more dangerous when the rotor operates near critical speeds, where resonance conditions amplify oscillations. Given these risks, a comprehensive understanding of rotordynamic behaviour is essential. It plays a vital role not only in reducing vibration-induced noise but also in preventing sudden and catastrophic failures of the rotating components, which could result in costly downtime and repairs.

Addressing these challenges in the design phase is even more important, as it allows engineers to predict potential problems before the machinery is manufactured and put into operation. One of the principal factors influencing the rotordynamic behaviour of contemporary turbomachinery is the effect of induced forces and moments on narrow, fluid-filled annuli, such as those found in journal bearings, annular seals and balance pistons. In these components, motion-dependent forces and moments are induced on the rotor, either solely or as a combination of the hydrodynamic [1] or Lomakin effect [2], due to substantial pressure differences across the annulus. It is this pressure differential that gives rise to significant flow components observed in the pertinent machine elements, being either axial or radial, for instance in annular seals or thrust collars, or a combination of both, e.g. in balance pistons.

Maximilian M.G. Kuhr · Zhengzhong Gao · Peter F. Pelz
Chair of Fluid Systems, Technische Universität Darmstadt, 64287 Darmstadt, Germany
e-mail: maximilian.kuhr@tu-darmstadt.de; zhengzhong.gao@tu-darmstadt.de; peter.pelz@tu-darmstadt.de

Matthew Allen et al. (eds.), *Special Topics in Structural Dynamics & Experimental Techniques, Vol. 5*, Conference Proceedings of the Society for Experimental Mechanics Series, https://doi.org/10.13052/97887-438-0150-4_7

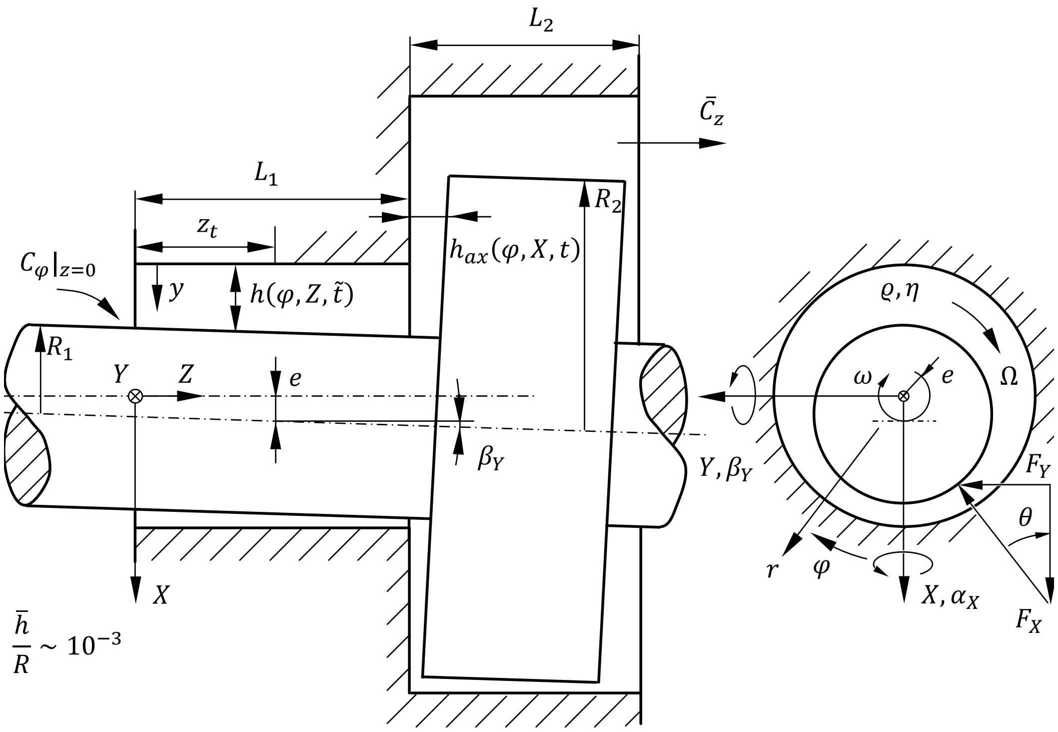

Fig. 1 Generic balance piston geometry.

While the force and moment characteristic of journal bearings or annular seals, with either a major axial or radial flow component is well-documented [3–8], the force and moment characteristic of machine elements with combined axial and radial flow such as balance pistons is largely unexplored due to the limited availability of reliable experimental data for validation purposes, cf. [9]. Furthermore, in examining the impact of annuli on overall machine dynamics, it is common practice to consider only the force characteristics due to lateral motions that are proportional to static and velocity-dependent movements of the rotor, i.e. the consideration of the annuli's stiffness and damping characteristics. However, when the complete equation of motion is considered, including the stiffnesses K, damping C and inertia M coefficients from the five degrees of freedom $X, Y, Z, \alpha_X, \beta_Y$,

$$-\begin{bmatrix} F_X \\ F_Y \\ F_Z \\ M_X \\ M_Y \end{bmatrix} = \begin{bmatrix} K_{XX} & K_{XY} & K_{XZ} & K_{X\alpha} & K_{X\beta} \\ K_{YX} & K_{YY} & K_{YZ} & K_{Y\alpha} & K_{Y\beta} \\ K_{ZX} & K_{ZY} & K_{ZZ} & K_{Z\alpha} & K_{Z\beta} \\ K_{\alpha X} & K_{\alpha Y} & K_{\alpha Z} & K_{\alpha\alpha} & K_{\alpha\beta} \\ K_{\beta X} & K_{\beta Y} & K_{\beta Z} & K_{\beta\alpha} & K_{\beta\beta} \end{bmatrix} \begin{bmatrix} X \\ Y \\ Z \\ \alpha_X \\ \beta_Y \end{bmatrix} + \begin{bmatrix} C_{XX} & C_{XY} & C_{XZ} & C_{X\alpha} & C_{X\beta} \\ C_{YX} & C_{YY} & C_{YZ} & C_{Y\alpha} & C_{Y\beta} \\ C_{ZX} & C_{ZY} & C_{ZZ} & C_{Z\alpha} & C_{Z\beta} \\ C_{\alpha X} & C_{\alpha Y} & C_{\alpha Z} & C_{\alpha\alpha} & C_{\alpha\beta} \\ C_{\beta X} & C_{\beta Y} & C_{\beta Z} & C_{\beta\alpha} & C_{\beta\beta} \end{bmatrix} \begin{bmatrix} \dot{X} \\ \dot{Y} \\ \dot{Z} \\ \dot{\alpha}_X \\ \dot{\beta}_Y \end{bmatrix} + \begin{bmatrix} M_{XX} & M_{XY} & M_{XZ} & M_{X\alpha} & M_{X\beta} \\ M_{YX} & M_{YY} & M_{YZ} & M_{Y\alpha} & M_{Y\beta} \\ M_{ZX} & M_{ZY} & M_{ZZ} & M_{Z\alpha} & M_{Z\beta} \\ M_{\alpha X} & M_{\alpha Y} & M_{\alpha Z} & M_{\alpha\alpha} & M_{\alpha\beta} \\ M_{\beta X} & M_{\beta Y} & M_{\beta Z} & M_{\beta\alpha} & M_{\beta\beta} \end{bmatrix} \begin{bmatrix} \ddot{X} \\ \ddot{Y} \\ \ddot{Z} \\ \ddot{\alpha}_X \\ \ddot{\beta}_Y \end{bmatrix}, \tag{1}$$

it becomes evident that the overall impact of the annuli may be more significant than initially expected when modelled, cf. [10]. It can be reasonably deduced that the modelling of the rotordynamic influence of the fluid-filled gaps is significant, particularly around critical rotation speeds. Within equation 1 F_X, F_Y, F_Z and M_X, M_Y are the induced forces and moments of the annulus acting on the rotor. The translational motion, velocity and acceleration of the rotor is given by $X, \dot{X}, \ddot{X}$, $Y, \dot{Y}, \ddot{Y}$, $Z, \dot{Z}, \ddot{Z}$ whereas $\alpha_X, \dot{\alpha}_X, \ddot{\alpha}_X$ and $\beta_Y, \dot{\beta}_Y, \ddot{\beta}_Y$ denotes the angular motion, velocity and acceleration of the rotor around the X and Y axis. The dependence on the Z coordinate is only pertinent in the context of a balance piston, as considered here. In the case of purely axial or purely radial flow through the gap, the equation of motion reduces accordingly.

Equation 1 can be written in an alternative form with the definition of the individual sub-matrices based on the four different combinations: (I) induced forces on the rotor from translational motion, (II) induced forces on the rotor from angular motion, (III) induced moments on the rotor from translational motion and (IV) induced moments on the rotor from angular motion

$$-\begin{bmatrix} F_X \\ F_Y \\ F_Z \\ M_X \\ M_Y \end{bmatrix} = \begin{bmatrix} \boldsymbol{K}_{\mathrm{I}} & \boldsymbol{K}_{\mathrm{II}} \\ \boldsymbol{K}_{\mathrm{III}} & \boldsymbol{K}_{\mathrm{IV}} \end{bmatrix} \begin{bmatrix} X \\ Y \\ Z \\ \alpha_X \\ \beta_Y \end{bmatrix} + \begin{bmatrix} \boldsymbol{C}_{\mathrm{I}} & \boldsymbol{C}_{\mathrm{II}} \\ \boldsymbol{C}_{\mathrm{III}} & \boldsymbol{C}_{\mathrm{IV}} \end{bmatrix} \begin{bmatrix} \dot{X} \\ \dot{Y} \\ \dot{Z} \\ \dot{\alpha}_X \\ \dot{\beta}_Y \end{bmatrix} + \begin{bmatrix} \boldsymbol{M}_{\mathrm{I}} & \boldsymbol{M}_{\mathrm{II}} \\ \boldsymbol{M}_{\mathrm{III}} & \boldsymbol{M}_{\mathrm{IV}} \end{bmatrix} \begin{bmatrix} \ddot{X} \\ \ddot{Y} \\ \ddot{Z} \\ \ddot{\alpha}_X \\ \ddot{\beta}_Y \end{bmatrix}. \tag{2}$$

Typically, the rotordynamic coefficients depend on three different characteristics of the annulus, cf. figure 1: (i) the geometry of the annular gap, i.e. the gap lengths L_i, the shaft radii R_i, the mean gap clearances $\bar{h}_i$ and the gap functions $h = h(\varphi, Z, t)$ respectively $h_{ax} = h_{ax}(\varphi, X, t)$ with the circumferential and axial coordinate φ, Z and the radial coordinate X; (ii) the operating conditions, i.e. the eccentric and angular position of the shaft e, α_X, β_Y, the distance of the centre of rotation z_T from the annulus entrance, the mean axial velocity $\bar{C}_z$, the angular velocity of the shaft Ω and the pre-swirl velocity at the annulus inlet $C_\varphi|_{z=0}$; (iii) the lubricant characteristics, i.e. the dynamic viscosity η and the fluid density ϱ.

To address the issue of a lack of experimental validation data, a revised test rig [7] developed by the Chair of Fluid Systems at the Technische Universität Darmstadt for the determination of the static and dynamic characteristics of annular gaps with combined axial and radial flow components is described in the following section. Due to the construction of a new rotor, a rotordynamic analysis is conducted on the test rig employing the Finite Element Method with the use of ANSYS Mechanical. During the analysis, not only is the rotor investigated in terms of eigenfrequencies and stability margin, but also the degrees of modelling the influence of the balance piston is examined.

Revised Annular Seal and Bearing Test Rig

The upper part of figure 2 shows the formerly presented test rig by Kuhr et al. & Kuhr [7, 11]. As illustrated, the main components of the test rig are the foundation, the motor, the axial bearing, the gap module as well as the two active magnetic bearings (AMB) to support and excite the rotor. Compared to conventional bearings such as ball or journal bearings used by several authors, cf. Childs [3, 12], Kanemori & Iwatsubo [13, 14] and Moreland et al. [15], magnetic bearings have the advantage of bearing the rotor completely contactless and thus frictionless. Furthermore, the AMBs constitute an intrinsic force and displacement measuring system, with the capability to excite the rotor radially at defined amplitudes and frequencies. This renders them particularly suited to the identification of the dynamic characteristics of rotating machinery and components such as annular seals and journal bearings. The test rig is capable of measuring both concentric and off centred, i.e. eccentric, as well as misaligned rotor positions in an eccentricity and misalignment range of $\varepsilon := e/\bar{h} = 0..0.9, \alpha_x, \beta_y = 0.15°$. By using a ten-stage centrifugal pump to supply the test rig, the axial pressure difference across the annuls Δp can be varied continuously in the range of $\Delta p = 0..20\,\mathrm{bar}$, whereas the pre-swirl at the seal entrance can be controlled in the range of $C_\varphi\big|_{z=0} = 0..1.7$. For further information on the capabilities, calibration and uncertainty of the test rig, please refer to the work of Kuhr [7] and Kuhr et al. [11].

The lower part of figure 2 illustrates the revised test rig for the identification of balance pistons, thrust collars and axial hydrodynamic bearings. In addition to larger and more powerful magnetic bearings, the axial bearing, the gap module and the rotor underwent significant modifications and redesign. Given the absence of an axial excitation of the rotor in previous designs, the axial bearing was created with the specific purpose of exciting the rotor in the axial direction. This is achieved through the use of a piezoelectric actuator with a possible displacement of $0.2\,\mathrm{mm}$ in combination with a movable axial bearing supported by linear guideways. The induced axial forces exerted by the balance piston are measured through the use of a piezoelectric force transducer with a measurement range of $\pm 14\,\mathrm{kN}$ and an absolute uncertainty of $\delta_F < 70\,\mathrm{N}$. At the same time, the induced moments of the annulus are supported by the magnetic bearings.

Figure 3 shows a technical drawing of the main part of the test rig, i.e. the gap module. The fluid path through the gap module is indicated by the black arrows. The module consists of 4 components: (i) the inlet to guide the flow and to measure the pre-swirl as well as the static pressure at the entrance of the annulus; (ii) the gap module; (iii) the outlet and (iv) the mechanical seals. The inlet is specifically designed to generate pre-swirled flows in front of the annulus. It is well known that the pressure field inside the annulus is influenced by the pre-swirl $C_\varphi\big|_{z=0}$. To investigate and quantify the influence on the static and dynamic characteristics, the process fluid, i.e. water, is tangentially fed into the inlet. By dividing the flow into two parts, the gap and the bypass volume flow, the circumferential velocity component in front of the annulus can be

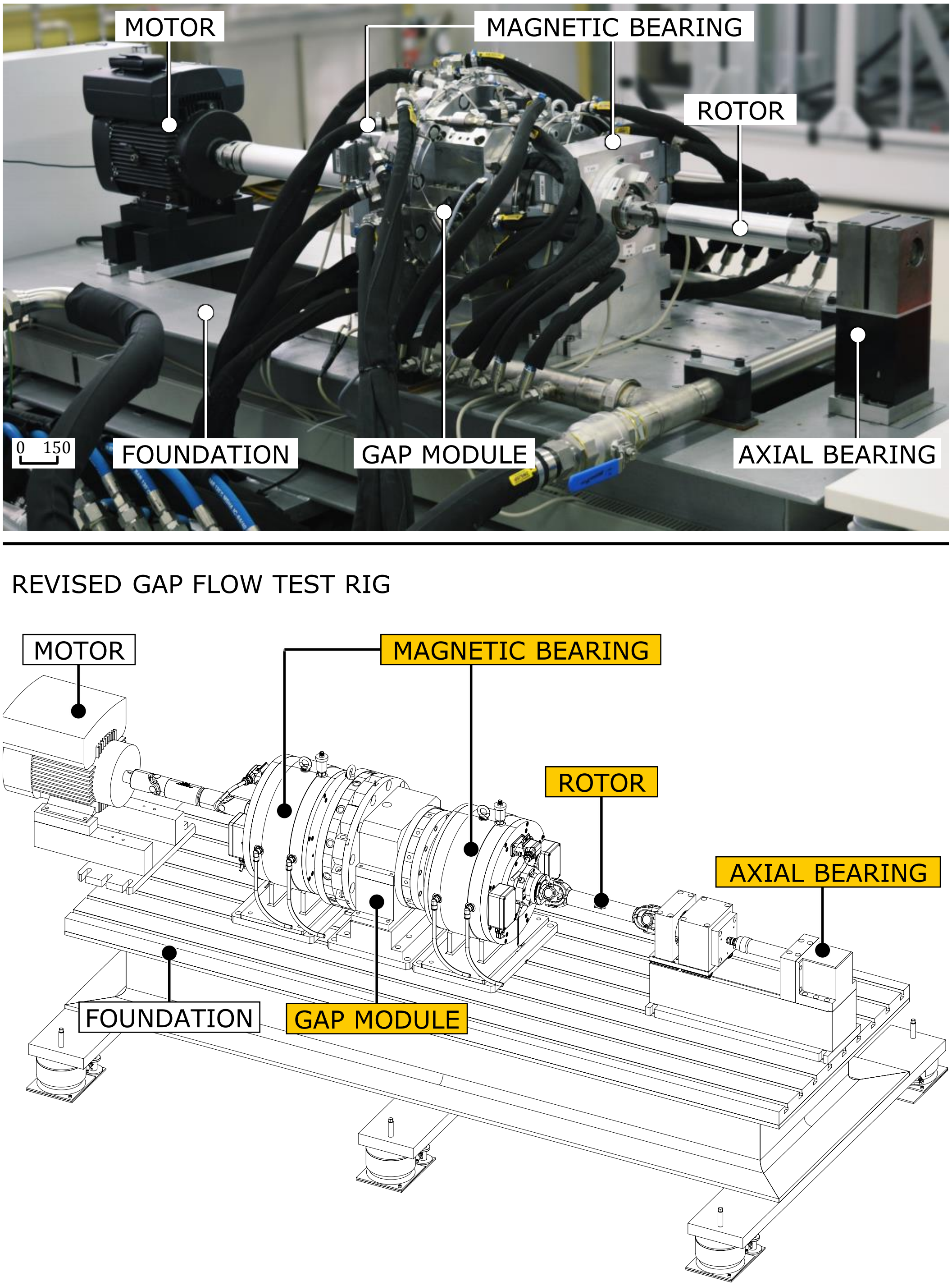

Fig. 2 Upper: Gap flow test rig at the Chair of Fluid Systems [7]; Lower: Revised test rig for the identification of annular gas with combined axial and radial flow component. The highlighted descriptions indicate major changed in the setup.

varied continuously. A Pitot tube connected to a pressure transmitter ($\delta_{\Delta p} < 0.01\,\mathrm{bar}$) is used to measure the circumferential velocity component. The test rig is capable of generating a pre-swirl in the range of $C_\varphi\big|_{z=0} = 0\,..\,1.7$. In order to ascertain the position of the rotor within the balance piston, the position of the shaft is measured at three distinct planes. (i) at the entrance, (ii) at the exit of the lubrication gap and (iii) at the midpoint of the thrust collar. To achieve this, two eddy current sensors are employed, each with a user-defined measuring range of $1\,\mathrm{mm}$ and an absolute uncertainty of $\delta_{X,\mathrm{GAP}} < \pm 2.4\,\mu\mathrm{m}$.

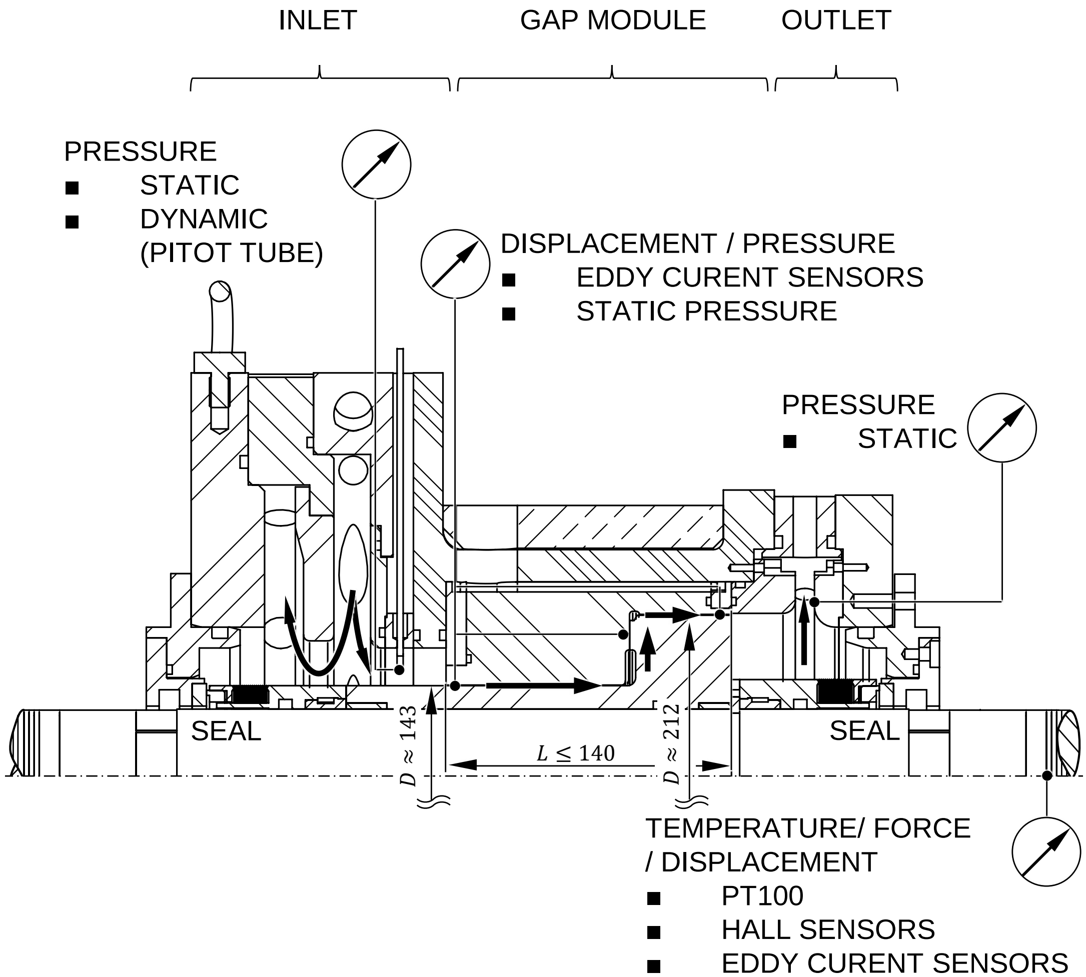

Fig. 3 Revised gap module of the annular seal and bearing test rig at the Chair of Fluid Systems. The black arrows indicate the flow path through the annulus inside the test rig.

These are arranged at an angle of 90° at the inlet and outlet of the piston. The axial position is then measured at four circumferentially distributed locations using identical eddy current sensors. Due to the modular design of the test rig, it is possible to vary the length of the piston as well as the clearance by changing the stator inlay and the rotor diameter within the gap module. The length can be varied in a range of $10\,\mathrm{mm} \leq L \leq 140\,\mathrm{mm}$, whereas the gap clearance varies between $0.1\,\mathrm{mm}$ and $0.7\,\mathrm{mm}$. The supply pressure is measured at the inlet of the gap module by using a pressure transmitter connected to four wall pressure taps equally space around the annulus with an uncertainty of $\delta_{p,z=0} < \pm 0.033\,\mathrm{bar}$. The static pressure before and after the thrust collar is determined using pressure transmitters connected to a single wall pressure tap, each, whereas the pressure difference across the annulus is measured by a differential pressure sensor with an absolute uncertainty of $\delta_{\Delta p} < \pm 0.04\,\mathrm{bar}$. The test rig is designed to investigate pressure differences of up to $20\,\mathrm{bar}$. The volume flow through the gap is measured using an electromagnetic flowmeter with an absolute uncertainty of $\delta_{\dot{Q},\mathrm{GAP}} < \pm 0.04\,Q_{\mathrm{GAP}}$. To avoid cavitation within the annulus, the test rig can be pressurised up to $15\,\mathrm{bar}$. The test rig is operated using water at a constant temperature of $35\,^{\circ}\mathrm{C}$ and is fed by a 10 staged $55\,\mathrm{kW}$ centrifugal pump.

Finally, figure 4 presents an isometric sketch of the revised rotor. The rotor is constructed from steel type 1.1730 and stainless-steel type 1.4305, comprising two cardanic shafts with preloaded needle bearings and the main rotor with the annular gap specimen and the rotating part of the mechanical face seals. The cardanic shafts have been selected on the basis of a carefully considered design. One shaft incorporates a slider mechanism, which serves to compensate for the axial excitations. In contrast, the other shaft is devoid of this feature. This design choice is crucial, as the induced axial forces are transmitted through the cardanic shaft without a slider into the aforementioned axial bearing, which is connected to the force transducer and the piezoelectric actuator. Additionally to the components of the rotor, figure 4 indicates the modelling of

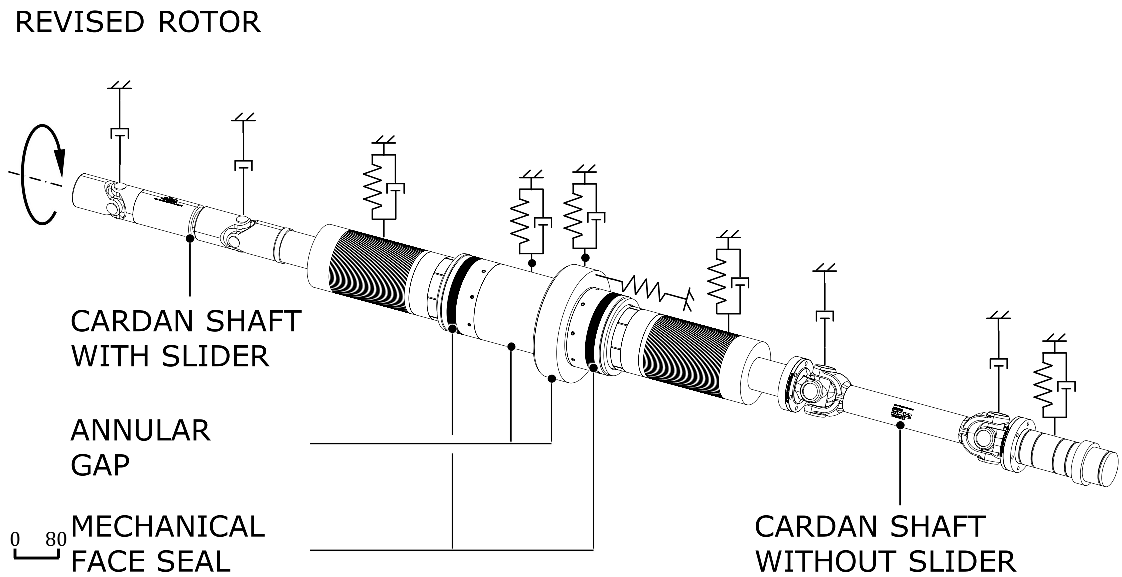

Fig. 4 Revised rotor of the annular seal and bearing test rig at the Chair of Fluid Systems. The sketched mechanical elements indicate the position of additional modelled stiffness, damping, and inertia coefficients used in the calculation.

the cardanic shaft joints, magnetic bearing, ball bearing and balance piston for the rotordynamic analysis. Here, the cardanic shaft joints are represented by assuming solely damping characteristics, whereas the magnetic bearings and ball bearings in the revised axial bearing are modelled using stiffness and damping coefficients. The annular gap of the balance piston is modelled by the aforementioned rotordynamic stiffness, damping and inertia coefficients, cf. equation 1. The material damping is chosen accordingly to the Rayleigh damping to be proportional to the mass and stiffness matrix, cf. Markert [16]

Results and Discussion

Numerical Setup

The rotordynamic analysis, in terms of predicting natural frequencies and stability margin, is carried out using a Finite Element Method (FEM) calculation using ANSYS Mechanical 2022 R2. Adjacent components with no relative motion are meshed and very fine structures with limited influence on the overall behaviour such as screws, holes and chamfers are neglected. The rotor was discretised using SOLID186 and SOLID187 elements, with element sizes ranging from 3 to 6 mm. Most of the components, such as those with cylindrical shapes, are meshed with hexagonal SOLID186 elements, while the components with more complicated geometries, such as the crossed cylinders in the universal joint, are meshed with SOLID187 elements, a high-order 3D element. The FEM simulation consists of approximately 550,000 nodes and 130,000 elements in total. COMBIN40 elements are used to model the deep groove ball bearings and the magnetic bearings. The COMBIN40 element is a combination of a spring and a damper in parallel and connects two nodes, one of which can be fixed to the ground. In the simulation, the outer ring of the bearing is assumed to be fixed to the ground, while the inner ring of the bearing is meshed with several nodes. These nodes are connected to one of the nodes of the COMBIN40 element using an MPC184 element, which indicates the multipoint constraint and models the kinematic constraints between the nodes. The MPC184 element is also used to model the coupling and translational joint. The inertia part of the dynamic coefficients is modelled by MASS21 elements, which are concentrated mass component elements with a single node. However, the MASS21 element cannot model the cross-coupled terms in the inertia matrices. As a result, only the diagonal terms of the inertia matrices are considered in the following calculation. The dynamic behaviour of the annular gap, i.e. the balance piston, is modelled using MATRIX27 elements. The values are obtained by an in-house calculation tool, the Clearance-Averaged Pressure Model for gaps with purely axial flow, see [6]. The influence of the thrust collar is obtained by CFD analysis. Only the direct stiffness K_{ZZ} is considered. Furthermore, the MATRIX27 element is only capable of modelling skew-symmetric inertia matrices. Therefore, the inertia matrices are only considered with the dominant diagonal terms. The complete equation of motion is reduced accordingly

$$
-\begin{bmatrix} F_X \\ F_Y \\ F_Z \\ M_X \\ M_Y \end{bmatrix} = \begin{bmatrix} K_{XX} & K_{XY} & 0 & K_{X\alpha} & K_{X\beta} \\ K_{YX} & K_{YY} & 0 & K_{Y\alpha} & K_{Y\beta} \\ 0 & 0 & K_{ZZ} & 0 & 0 \\ K_{\alpha X} & K_{\alpha Y} & 0 & K_{\alpha\alpha} & K_{\alpha\beta} \\ K_{\beta X} & K_{\beta Y} & 0 & K_{\beta\alpha} & K_{\beta\beta} \end{bmatrix} \begin{bmatrix} X \\ Y \\ Z \\ \alpha_X \\ \beta_Y \end{bmatrix} + \begin{bmatrix} C_{XX} & C_{XY} & 0 & C_{X\alpha} & C_{X\beta} \\ C_{YX} & C_{YY} & 0 & C_{Y\alpha} & C_{Y\beta} \\ 0 & 0 & 0 & 0 & 0 \\ C_{\alpha X} & C_{\alpha Y} & 0 & C_{\alpha\alpha} & C_{\alpha\beta} \\ C_{\beta X} & C_{\beta Y} & 0 & C_{\beta\alpha} & C_{\beta\beta} \end{bmatrix} \begin{bmatrix} \dot{X} \\ \dot{Y} \\ \dot{Z} \\ \dot{\alpha}_X \\ \dot{\beta}_Y \end{bmatrix}
$$
$$
+ \begin{bmatrix} M_{XX} & & & & \\ & M_{YY} & & & \\ & & 0 & & \\ & & & M_{\alpha\alpha} & \\ & & & & M_{\beta\beta} \end{bmatrix} \begin{bmatrix} \ddot{X} \\ \ddot{Y} \\ \ddot{Z} \\ \ddot{\alpha}_X \\ \ddot{\beta}_Y \end{bmatrix}, \tag{3}
$$

$$
-\begin{bmatrix} F_X \\ F_Y \\ F_Z \\ M_X \\ M_Y \end{bmatrix} = \begin{bmatrix} K_I & 0 & K_{II} \\ 0 & K_{ZZ} & 0 \\ K_{III} & 0 & K_{IV} \end{bmatrix} \begin{bmatrix} X \\ Y \\ Z \\ \alpha_X \\ \beta_Y \end{bmatrix} + \begin{bmatrix} C_I & 0 & C_{II} \\ 0 & 0 & 0 \\ C_{III} & 0 & C_{IV} \end{bmatrix} \begin{bmatrix} \dot{X} \\ \dot{Y} \\ \dot{Z} \\ \dot{\alpha}_X \\ \dot{\beta}_Y \end{bmatrix} + \begin{bmatrix} M_I & & \\ & 0 & \\ & & M_{IV} \end{bmatrix} \begin{bmatrix} \ddot{X} \\ \ddot{Y} \\ \ddot{Z} \\ \ddot{\alpha}_X \\ \ddot{\beta}_Y \end{bmatrix}. \tag{4}
$$

Campbell Diagram
Influence of Different Levels of Modelling the Dynamics of the Annulus

The eigenfrequency analysis is carried out in the operating range of the test rig. Here, the rotor speed can be varied from a minimum of $f = 6.3$ to a maximum of $50\,\mathrm{Hz}$, whereas the pressure difference across the balance piston is assumed to be constant at a value of $\Delta p = 10\,\mathrm{bar}$. The balance piston itself consists of three separate gaps, (i) a first annular gap with a relative length of $L_1/R_1 = 1.26$ and a relative clearance of $\bar{h}_1/R_1 = 1.7\,‰$, (ii) the thrust collar with an assumed gap height of $\bar{h}_{ax} = 0.1\,\mathrm{mm}$ and (iii) a second annular gap with a relative length of $L_1/R_1 = 0.47$ and a relative clearance of $\bar{h}_1/R_1 = 2.6\,‰$. This results in circumferential Reynolds numbers of the annuli of $Re_{\varphi,1} := (\Omega R_1 \bar{h}_1)/\nu \approx 750..5889$ and $Re_{\varphi,2} := (\Omega R_2 \bar{h}_2)/\nu \approx 1800..12000$, indicating both laminar and turbulent flow conditions over the rotor speed range. Six different degrees of modelling the influence of the balance piston is investigated:

(a) Only the rotor system and its foundations are modelled, i.e. the rotor is operated without the balance piston.
(b) The rotor system and the stiffness and damping coefficients due to translational motion, i.e. K_I and C_I, are considered.
(c) The rotor system as well as the stiffness, damping and inertia coefficients due to translational motion, i.e. K_I, C_I and M_I, are considered.
(d) The rotor system as well as the stiffness, damping and inertia coefficients of the forces due to translational and angular motion, i.e. $K_{I..II}$, $C_{I..II}$ and $M_{I..IV}$, are considered.
(e) The rotor system and the stiffness, damping and inertia coefficients of the forces and moments due to translational and angular motion, i.e. $K_{I..IV}$, $C_{I..IV}$ and $M_{I..IV}$, are considered.
(f) The rotor system and the full reduced matrix, equation 3, i.e. the stiffness, damping and inertia coefficients of the forces and moments due to translational and angular motion, as well as the direct axial stiffness K_{ZZ}, are taken into account.

Figure 5 depicts the Campbell diagrams of the six different degrees of modelling the influence of the balance piston, which illustrate the natural eigenfrequencies of the rotor system of the rotor speed for varying degrees of modelling. The black lines represent the rotor speed and twice the rotor speed, while the coloured lines correspond to the different eigenmodes of the rotor system. An intersection between the black and coloured lines indicates a critical speed of the system. In the figures, the first three bending modes, as well as the first torsional and first axial mode, are displayed. The solid lines represent a forward whirling motion of the rotor, whereas the dashed lines indicate a backward whirl. Distinction between forward and backward whirl is evident only for the different bending modes. Additionally, the critical speeds of the system are given in the figures. Here, the value is an approximate evaluation based on the forward whirl motion of the rotor.

Focussing first on the rotor without the liquid-filled balance piston (figure 5a), it becomes evident, that the most critical eigenmode is the second bending mode (blue line) as well as the first torsional mode (green) of the system. Both modes occur initially above twice the rotational frequency of the rotor. At a critical frequency of approximately 22 Hr and 44 Hz, the second bending mode coincides with twice the speed of the rotor as well as its actual speed, making it a critical point. The first axial mode as well as the third bending mode always lies above twice the speed of the rotor.

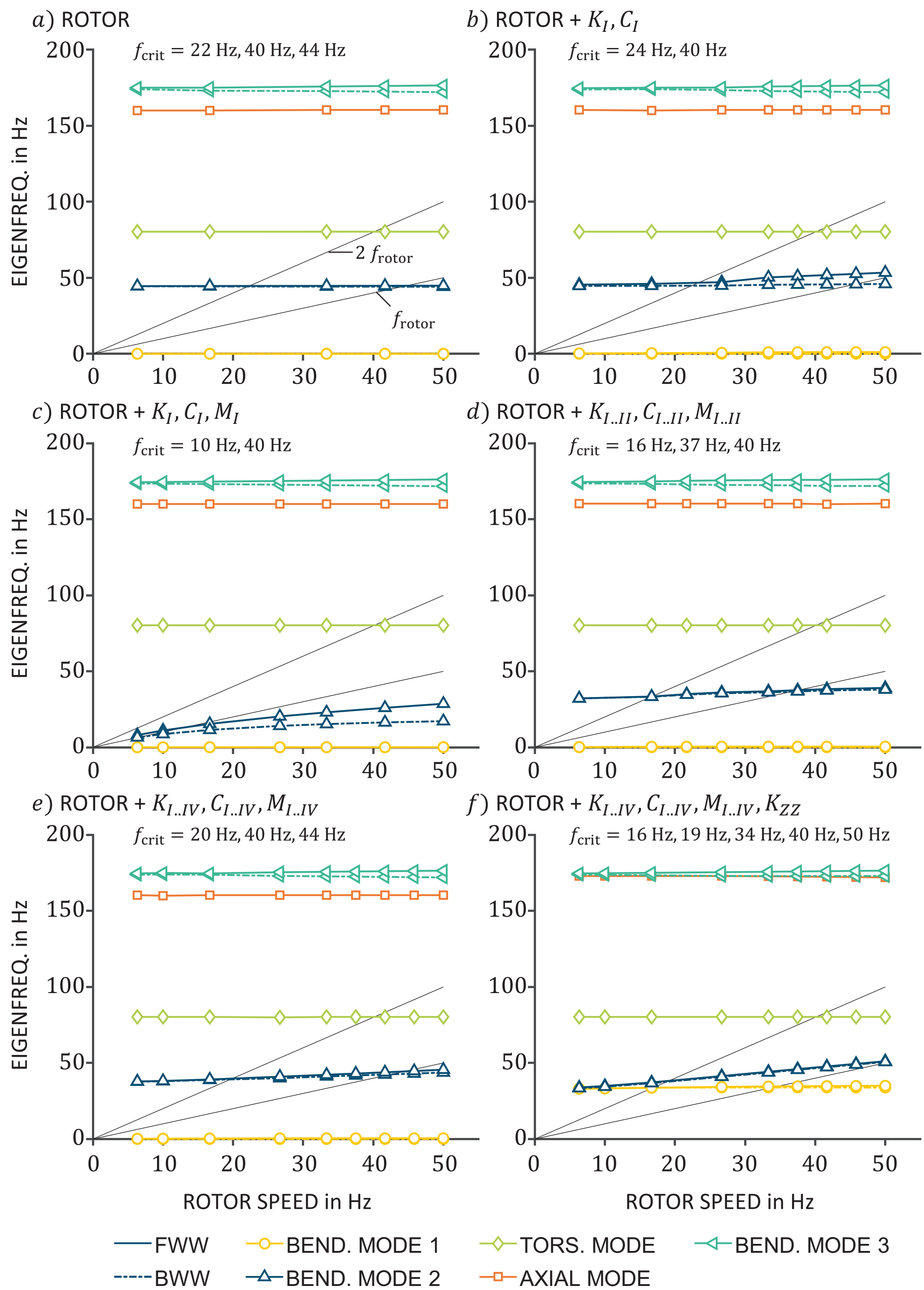

Fig. 5 Campbell diagrams of the rotor system. The different figures $a)$ to $f)$ indicate different degrees of modelling of the rotordynamic influence of the fluid-filled gaps, ranging from $a)$ the rotor without the annulus, to $f)$ the rotor with a balance piston inducing both forces and moments as well an additional axial stiffness onto the rotor

Focussing now on the impact of the annular gap and later the overall balance piston. Figure 5b depicts the Campbell diagram when the rotor system and the stiffness and damping coefficients due to translational motion, i.e. K_I and C_I, are considered. This level of modelling is typically employed for classical journal bearings with laminar flow conditions, where the influence of flow inertia is negligible. It is shown that there is only a slight change in the eigenfrequencies of the overall rotor - gap system. The first bending mode is almost unaltered, whereas the eigenfrequencies of the second bending mode experience a slight increase towards higher rotor speeds. Due to this increase, the forwards whirling motion of the second bending mode is no longer a critical frequency at a spinning speed of 44 Hz. Furthermore, the frequency difference between the forward and backward whirl motion is more pronounced at rotor speed exceeding 25 Hz. The introduction of the annulus has no impact on the first torsional mode as well as on the first axial mode and the third bending mode. By introducing the annular gaps, the rotor balance piston system exhibits three critical speeds over the operation range of the test rig.

Focussing now on the impact of the additional inertia coefficients M_I of the balance piston, figure 5c a strong decrease of the eigenfrequencies of the second bending mode. This is reasonable since adding additional mass terms, like the added mass induced by the annulus, lowers the eigenfrequencies of the oscillating system. This is of peculiar interest, as the reduction in frequency is proportional to the increased mass. It is important to recognise that the masses induced by the annular gap, especially with an eccentric rotor, can be an order of magnitude higher than the mass of the rotor itself. In the case shown here, the added mass of the balance piston is approximately equal to the mass of the solid rotor. Nevertheless, it is essential to consider the added mass when assessing the natural frequencies of the overall system.

The aforementioned trend of nearly unrecognisable changes in the Campbell diagram is also apparent when considering not only the stiffness, damping and inertia resulting from forces due to translational movements but also the coefficients of forces resulting from angular motions, i.e. K_{II}, C_{II} and M_{II}, cf. figure 5d. Nevertheless, a more detailed examination reveals a notable discrepancy. On the one hand, the system now exhibits three critical frequencies when the coefficients K_{II}, C_{II} and M_{II} are considered. This was first the case when only considering the rotor, cf. figure 5a. On the other hand, the resonance frequency of the second bending mode (blue) exhibits a slight shift towards lower frequencies. This phenomenon can be attributed to the fact that the second bending mode represents an S-shaped movement, i.e. a tumbling movement within the annular gap. It is therefore to be expected that this motion will be influenced by the angular stiffness, damping and inertia of the gap. Regarding the first torsional and axial mode as well as the third bending mode, no significant changes can be seen.

Finally, figure 5e and 5f show the impact of the induced moments of the annulus on the eigenfrequencies of the systems. Similar to the figures above, the visible changes in figure 5e are small. However, when taking all rotordynamic coefficients into account, the first and second bending mode are altered as well as the axial mode. Furthermore, the number of critical speeds of the system increased to five critical speeds. However, the underlying reasons for the significant alterations observed in the initial bending mode remain to be fully elucidated.

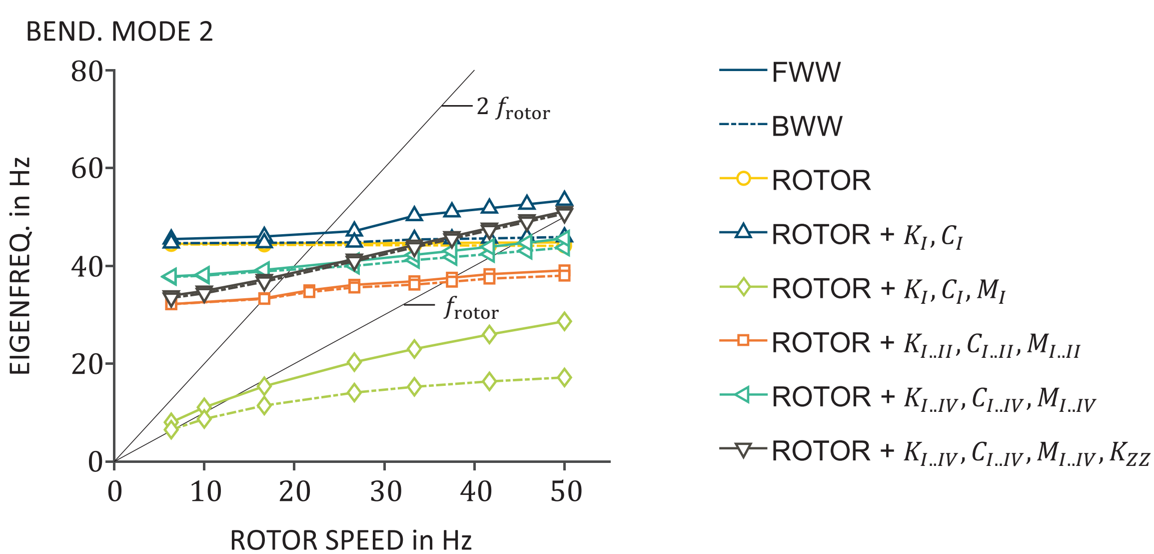

Fig. 6 Detailed investigation of the first and second bending mode regarding the influence of the different degrees of modelling of the rotordynamic influence of the balance piston.

In order to emphasise the impact of the different degrees of modelling the rotordynamic impact of the balance piston on the test rig rotor, the second bending mode is displayed in detail in figure 6. In contrast to figure 5, the different coloured lines represent the different degrees of modelling the impact of the annulus. The second bending mode of the rotor exerts a significant impact on the selection of stiffnesses, damping, and inertia coefficients. As the level of detail in the dynamic characteristic of the balance piston increases, the resonance frequency of the second bending mode increases at first, but

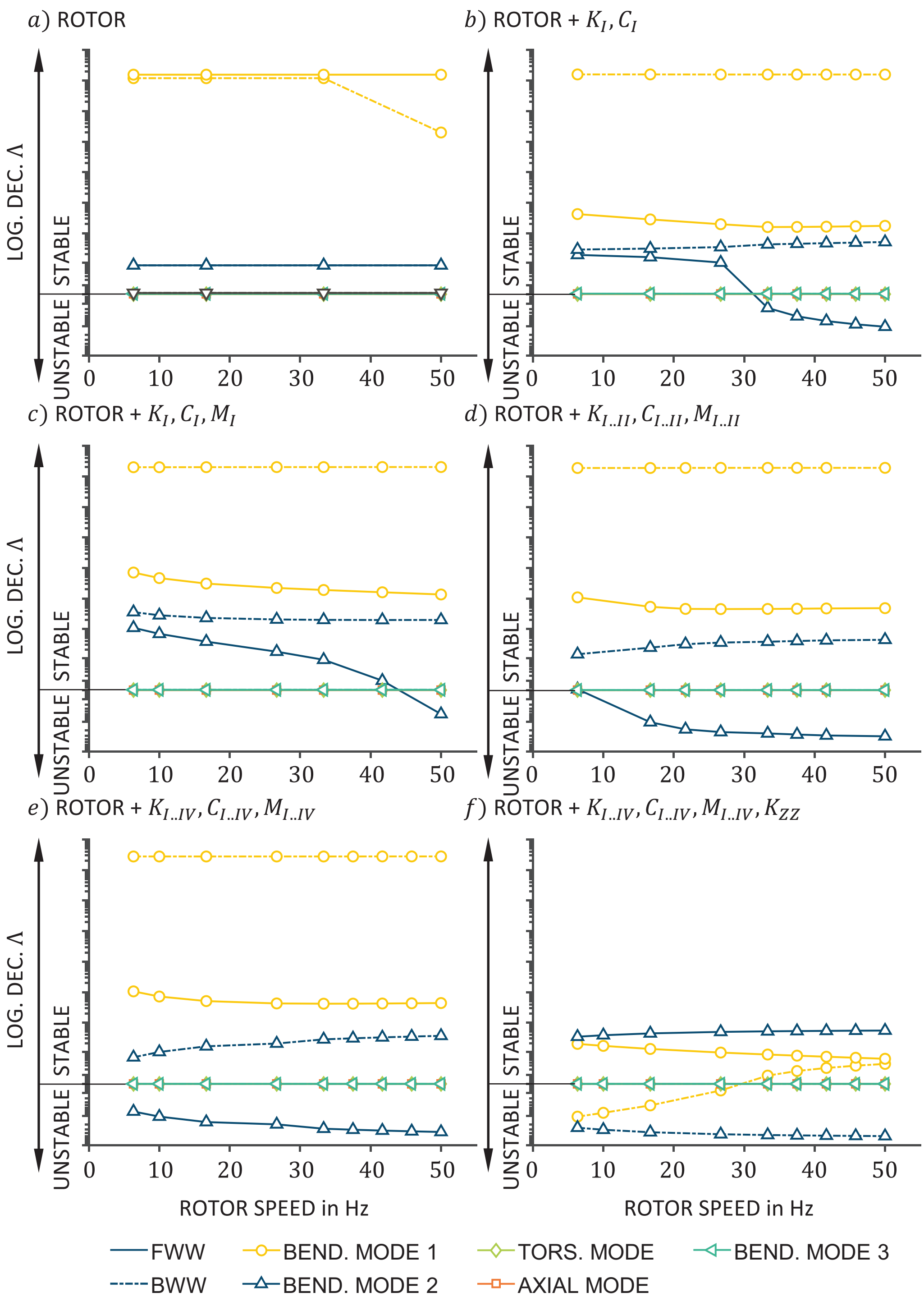

Fig. 7 Stability diagram of the rotor system. The different figures $a)$ to $f)$ indicate different degrees of modelling of the rotordynamic influence of the fluid-filled gaps, ranging from $a)$ the rotor without the annulus, to $f)$ the rotor with a balance piston inducing both forces and moments as well an additional axial stiffness onto the rotor.

decreases significantly when adding the added mass to the calculations. Subsequently, the eigenfreqeuncies increase with the detail in modelling. Intrestingly, when taking all rotordynamic influences into account, the second bending mode exhibits a characteristic similar to the system when only taking the stiffness and damping coefficients due to the translational motion into account.

Stability Analysis

To provide a comprehensive analysis, the stability of the system is evaluated using the logarithmic decrement. A positive logarithmic decrement indicates a stable eigenvalue and, consequently, a stable system. Conversely, a negative logarithmic decrement signifies an unstable eigenvalue, which in turn denotes an unstable system. The logarithmic decrement can be interpreted physically by considering the time course of a decaying oscillation in a weakly damped system. The ratio of two consecutive oscillation amplitudes, $q(t)$ and $q(t+\Delta t)$, which are offset by the time Δt, is

$$\frac{q(t)}{q(t+\Delta t)} = \exp\left(\Lambda\right). \tag{5}$$

The logarithmic decrement Λ is defined as the exponent of the ratio of two successive oscillations. If the exponent is negative, the amplitudes will increase over time. Conversely, if the exponent is positive, then the oscillations decay over time. Therefore, a negative logarithmic decrement is indicative of unstable system behaviour, whereas a positive logarithmic decrement signifies a stable state of the system. It should be noted that the logarithmic decrement is only defined for weakly damped systems.

Figure 7 depicts the stability diagrams of the six different degrees of modelling the influence of the balance piston. In contrast to the Campbell diagram, the black line represents the stability threshold at which the system modes become unstable. As with the analysis of the critical frequencies, the stability diagrams demonstrate a significant impact of the degree of modelling on the dynamic characteristics of the balance piston. The introduction of the annulus results in a modification of the overall rotor system, cf. figure 7a. The forward whirl motion of the second bending mode becomes unstable, whereas the first bending mode is stable over the pictured rotor speeds. Interestingly, the second bending mode is also the one influenced the most when increasing the degree of modelling the rotordynamic influence of the balance piston. It is also worth noticing that the characteristic changes when taking the axial stiffness of the balance piston K_{ZZ} into account, cf. figure 7f. Here, the forward whirl motions of the second bending mode becomes stable.

Interestingly, and in contrast to the Campbell diagrams in the previous chapter, clear differences in the stability of the system can be observed as the level of detail of the modelling increases. For example, figure 7d shows that adding the stiffness, damping and inertia coefficients of the forces induced by the angular motion, K_{II}, C_{II} and M_{II}, destabilises the forward whirl motion of the second bending mode, even at small rotor frequencies. This becomes even more pronounced when taking the induced moments due to the translational and angular motion into account, cf. figure 7e. However, at the finest level of modelling, the system seems to be stable for all the investigated forward whirl motion. The results of the stability analysis reinforce the conclusion of the Campbell diagrams that the extent to which annular gap flows are modelled, namely the degree to which coefficients representing forces and moments due to translational and angular motion are included, has a considerable impact on the overall dynamic behaviour of the system, particularly regarding the stability margin of critical frequencies.

Summary & Conclusion

The performance of rotating machinery, such as compressors or turbo pumps, is significantly affected by the dynamic characteristics of narrow fluid-filled gaps. These include media- or oil-lubricated journal bearings, annular seals, thrust bearings and balance pistons. In particular, the dynamic characteristic of annuli with combined axial and radial flow components such as balance pistons is not yet fully understood. Therefore, a revised annular seal and bearing test rig is resented. The revised rotor is subjected to rotordynamic analysis, with a particular focus on eigenfrequencies and system stability. Furthermore, the impact of the level of modelling the rotordynamic characteristic of balance pistons is examined. In particular, we are examining the impact of added mass, as well as the effects of additional stiffness and damping resulting from induced forces or moments due to translational and angular degrees of freedom. The introduction of stiffness, damping, and inertia coefficients related to both translational and angular motions has a significant impact on the system's natural frequencies and critical speeds, particularly affecting mainly the second bending mode. As the level of detail in the modelling increases, the resonance frequencies of this mode shift, notably exhibiting both an increase as well a decrease in the eigenfrequencies. This highlights the necessity of considering not only the translational effects, but also the angular forces and moments induced by the balance piston and annular gaps in rotordynamic analyses. The findings indicate that conventional approaches that neglect these additional degrees of freedom could result in underestimations of critical speeds and unexpected large vibration amplitudes, particularly in turbomachinery systems operating near critical speeds.

CRediT Authorship Contribution Statement

Maximilian M.G. Kuhr:	Conceptualization, Methodology, Analysis, Validation, Investigation, Writing, Visualization, Supervision, Project Administration.
Zhengzhong Gao:	Software, Analysis, Validation, Investigation.
Peter F. Pelz:	Funding.

Acknowledgments The financial support of the Federal Ministry for Economic Affairs and Climate Action (BMWK) due to an enactment of the German Bundestag under Grant No. 03EE5127D and KSB SE & Co. KGaA is gratefully acknowledged.

References

1. Szeri, A.Z. *Fluid film lubrication: Theory and design*. Cambridge University Press, Cambridge (1998)
2. Lomakin, A.A. "Calculation of the critical speed and the conditions to ensure dynamic stability of the rotors in high pressure hydraulic machines, taking account of the forces in the seals (in russian).". *Energo Mashinostroinie*, 14(4):1–5 (1958)
3. Childs, D.W. *Turbomachinery rotordynamics: Phenomena, modeling, and analysis*. A Wiley Interscience publication. Wiley, New York (1993)
4. Tiwari, R., Lees, A.W., and Friswell, M.I. "Identification of dynamic bearing parameters: A review". *The Shock and Vibration Digest*, 36(2):99–124 (2004)
5. Tiwari, R., Manikandan, S., and Dwivedy, S.K. "A review of the experimental estimation of the rotor dynamic parameters of seals". *The Shock and Vibration Digest*, 37(4):261–284 (2005)
6. Kuhr, M.M.G., Nordmann, R., and Pelz, P.F. "Dynamic force and moment characteristics of annular gaps—simulation results and evaluation of the relevance of the tilt and moment coefficients". *Journal of Tribology*, 145(1):1–42 (2023)
7. Kuhr, M.M.G. "Identification of the dynamic force and moment characteristics of annular gaps using linear independent rotor whirling motions". *Mechanical Systems and Signal Processing*, 187:109936 (2023)
8. Kuhr, M.M.G. and Pelz, P.F. "Experimental identification of the force and moment characteristic of symmetrically and non-symmetrically profiled annular seals". *Bulletin of the Polish Academy of Sciences Technical Sciences*, 71(6):e147062 (2023)
9. Kim, H., Jang, G., and Lee, S. "Complete determination of the dynamic coefficients of coupled journal and thrust bearings considering five degrees of freedom for a general rotor-bearing system". *Microsystem Technologies*, 17(5-7):749–759 (2011)
10. Kuhr, M.M.G. *Dynamische Eigenschaften axial durchströmter Ringspalte*, volume Band 29 of *Forschungsberichte zur Fluidsystemtechnik*. Shaker Verlag, Düren, [1. auflage] edition (2022)
11. Kuhr, M.M.G., Lang, S.R., and Pelz, P.F. "Static force characteristic of annular gaps – experimental and simulation results". *Journal of Tribology*, 144(11):1–18 (2022)
12. Childs, D.W. and Hale, K. "A test apparatus and facility to identify the rotordynamic coefficients of high-speed hydrostatic bearings". *Journal of Tribology*, 116(2):337–343 (1994)
13. Kanemori, Y. and Iwatsubo, T. "Experimental study of dynamic fluid forces and moments for a long annular seal". *Journal of Tribology*, 114(4):773–778 (1992)
14. Kanemori, Y. and Iwatsubo, T. "Forces and moments due to combined motion of conical and cylindrical whirls for a long seal". *Journal of Tribology*, 116(3):489–498 (1994)
15. Alex Moreland, J., Childs, D.W., and Bullock, J.T. "Measured static and rotordynamic characteristics of a smooth-stator/grooved-rotor liquid annular seal". *Journal of Fluids Engineering*, 140(10) (2018)
16. Markert, R. *Strukturdynamik: Skript zur Vorlesung Strukturdynamik für Maschinenbauer*. Techn. Univ. Darmstadt Fachgebiet Strukturdynamik, Darmstadt, 1., verb. aufl. edition (2010)